# Zweitveröffentlichung/ Secondary Publication

Leticya Lais Coelho, Matthieu Grao,Thomas Pomone, Marina Ratova, Peter Kelly, Michaela Wilhelm, Regina de Fátima Peralta Muniz Moreira

## Photocatalytic microfiltration membranes produced by magnetron sputtering with self-cleaning capabilities

Recommended Citation (primary publication/Version of Record) incl. DOI:

Leticya Lais Coelho, Matthieu Grao, Thomas Pomone, Marina Ratova, Peter Kelly, Michaela Wilhelm, Regina de Fátima Peralta Muniz Moreira,
Photocatalytic microfiltration membranes produced by magnetron sputtering with self-cleaning capabilities,
Thin Solid Films, Volume 747, 2022, 139143, ISSN 0040-6090,
https://doi.org/10.1016/j.tsf.2022.139143

## Take down policy
If you believe that this document or any material on this site infringes copyright, please contact publizieren@suub.uni-bremen.de with full details and we will remove access to the material.

# Photocatalytic microfiltration membranes produced by magnetron sputtering with self-cleaning capabilities

Leticya Lais Coelho [a,c], Matthieu Grao [b], Thomas Pomone [b], Marina Ratova [b], Peter Kelly [b], Michaela Wilhelm [c], Regina de Fátima Peralta Muniz Moreira [a,*]

[a] *Federal University of Santa Catarina (UFSC), Department of Chemical and Food Engineering (EQA), 88040 900 Florianópolis, SC, Brazil*
[b] *Surface Engineering Group, Faculty of Science and Engineering, Manchester Metropolitan University, Chester Street, M1 5GD, UK*
[c] *University of Bremen, Advanced Ceramics, Am Biologischen Garten 2, IW3, 28359 Bremen, Germany*

## ABSTRACT

*Keywords:*
Photocatalysis
Magnetron sputtering
Membrane separation process
Membrane functionalization
Wastewater treatment

In the present work, asymmetric alumina flat membranes were coated with $TiO_2$ thin films of varying thickness for wastewater treatment application. The coating was produced by magnetron sputtering, a deposition technique of high industrial relevance which could enable high volume manufacturing of photocatalyst coated membranes. The photocatalyst was used against membrane fouling, by taking advantage of the self-cleaning capabilities of $TiO_2$ when irradiated by UV light. The morphology and pore size of the coated membranes was evaluated by scanning electron microscopy. The antifouling property of the photocatalyst was assessed against two pollutants, methylene blue (MB) in aqueous phase and soybean oily emulsion. Under ultraviolet irradiation, the coating was able to restore membrane flux by degrading the fouling formed by MB, with selectivity reaching up to 86% of MB removal for the thickest $TiO_2$ thin film. The thickness didn't appear to have a significant impact on the photocatalytic activity, but it was negatively correlated with pore size, which enables membrane pore size and selectivity to be tailored. In oily conditions, the photocatalyst was not able to prevent membrane fouling, which was attributed to fouling inside the pores, catalyst inactivation through the formation of an oil layer at its surface, and to a low radiant flux.

## 1. Introduction

The world faces severe pressure on clean water supplies, leading to serious environmental and population health problems [1,2]. Given the increasing amount and complexity of industrial effluents and the inefficiency of conventional water and wastewater treatment techniques in treating them properly, there is an urgent need for technologies to improve wastewater treatment, removing even trace amounts of toxic pollutants [2–6]. Membrane separation processes [2,7] and advanced oxidative processes such as photocatalysis [8–10] and hybrid systems [11–14] have emerged as important technologies to overcome such limitations.

Micro-, ultra- and nanofiltration membranes are physical selective porous barriers with progressively reduced pore sizes and a gradient pressure is used as driving force for filtration [15]. The membrane surface plays the role of selective barrier. Thus, membrane selectivity (separation capacity) is mainly governed by the relation between the pore size of the membrane surface and the size of the pollutant molecule.

Smaller pore sizes lead to higher selectivity but increase the flux resistances, which reduces the flux and leads to higher energy consumption [16,17]. Therefore, asymmetric membranes with a hierarchical porous structure composed of a porous support (mechanical resistance and high permeability) and one or several layers with gradient porosity (suitable surface pore size) have been developed to produce membranes with high permeability and selective [18–20]. It should also be noted that the effective membrane thickness may vary from the theoretical one, as it is based on a previous calibration made by deposition on a smooth substrate.

Despite the benefits and current importance, ceramic membranes still suffer from serious fouling problems. Fouling is a common process where species present in the filtration medium block pores by forming a cake-like layer on the membrane surface or depositing inside the pores, which hinders membrane flux [7]. Various strategies, including the use of Photocatalytic Membranes (PMs), have been investigated to produce membranes with antifouling or self-cleaning capabilities that could improve filtration performance and life span of the membrane and

reduce replacement costs [6,21–23,59,60]. Photocatalysis is based on the generation of high reactive radicals on a photocatalyst by a suitable luminous source. By using an efficient photocatalyst on the membrane surface exposed to the light, refractory or toxic compounds deposited on the membrane surface could be degraded and/or eliminated. Titania ($TiO_2$) is the most used photocatalyst, with the anatase phase generally considered more active than the rutile phase [24]. Under UV irradiation, $TiO_2$ PM could achieve an effective removal of organic matter such as dyes [25], phenol [26], oil [27], and emerging pollutants [28]. PMs can be produced by depositing an active layer on the membrane surface.

The deposition of a thin layer of photocatalyst is frequently done by sol-gel dip-coating [29] or chemical vapor deposition [30], but can also be done by physical vapor deposition, such as magnetron sputtering [31]. Magnetron sputtering is a plasma-based thin film deposition process used to produce a wide variety of metallic and ceramic coatings. It is reproducible, highly scalable, and provides excellent control over the chemical and morphological properties of the deposited materials [32]. Magnetron sputtering is an industrially-relevant method of choice to produce photocatalytic coatings as it provides reliable control of parameters such as crystallinity, composition, and thickness, is applicable for several types of photocatalysts and presents good adhesion [33]. Although it has been applied to several types of surfaces, photocatalytic membranes produced by this technique are scarce [17,31,34,35].

Sanchez et al [31]. have investigated photocatalytic ceramic membranes functionalized by magnetron sputtering. Nevertheless, self-cleaning properties were not evaluated and only nanofiltration membranes were used by the authors. Due to the high potential of such a hybrid system, further investigation should be performed to produce efficient, self-cleaning, and long-lasting membranes. In this sense, the objective of the present work was to evaluate the effect of varying the amount of deposited photocatalyst on microfiltration alumina membranes to produce photocatalytic membranes with tailored porosity and self-cleaning capabilities.

## 2. Material and methods

### 2.1. Membrane preparation

Alumina flat membranes (approximately 16 mm x 16 mm x 0.7 mm) with pore sizes suitable for microfiltration process, produced as previously reported [36] were coated with titanium dioxide thin films via pulsed Direct Current (pDC) reactive magnetron sputtering. The deposition process was performed under high vacuum, with a base pressure of $3 \times 10^{-3}$ Pa and a working pressure of $4.4 \times 10^{-1}$ Pa, achieved through a combination of rotary (BOC Edwards 80) and turbo-molecular (Leybold TMP1000) pumps. A single $300 \times 100$ mm titanium target (99.5% purity) was fitted onto a Gencoa Ltd unbalanced type II magnetron. The distance between the target and the substrate was set to 50 mm. The argon flow rate was maintained via mass-flow controller and kept constant at 50 sccm for all experimental runs. The oxygen flow was regulated by a Speedflo®™ controller from Gencoa Ltd to produce stoichiometric films and to minimize target poisoning. The magnetron was powered by an Advanced Energy Pinnacle Plus power supply in pDC mode operating at 1 kW, pulse frequency of 100 kHz, and 60% duty cycle.

The coating thickness was estimated by simultaneously depositing titanium dioxide on alumina membranes and flat microscope glass slide substrates under the same deposition conditions. The coating thickness on the glass slide was measured by creating an artificial step, by covering part of it with Kapton tape prior to the deposition. A Profilm3D interferometer from Filmetrics, with a magnification of 50x, was used to measure the height of the artificial step. Based on a previous calibration, coatings of 50, 200, and 400 nm of estimated thickness were deposited on membrane surfaces by varying the deposition time from 5 to 30 min. The films were annealed in air at 600 °C for 1 h in an electric furnace. Membranes here are denoted as "MS-*x* nm", where *x* relates to coating thickness.

Prior to filtration tests, membranes were cut in disks of 1 cm diameter (geometric area of filtration was 0.785 cm$^2$).

### 2.2. Membrane morphology and surface chemistry

Scanning electron microscopy images (SEM) (Zeiss Supra 40 VP-FEG-SEM) were performed at 2 kV and different magnifications using secondary electron mode. Electron dispersive spectroscopy (EDS) analysis (Tescan Vega-3 LMU coupled with a probe of energy-dispersive x-ray spectroscopy) were used to analyze the effect of the coatings in terms of surface morphology and composition. For EDS imaging, 15 mm of working distance, 15 kV voltage and 9 MV beam intensity were used. Average pore sizes of the surface were determined from SEM images (5000 × magnification) using a dedicated software (ImageJ) [36,37]. Raman spectroscopy (Anton Paar Cora 5200, integration time = 5000 ms, 250 mW784 nm, 5 scans for each sample) and X-ray diffraction (XRD) (PANalytical X`pert powder diffractometer with CuKa1 radiation (λ = 1.541 Å) were used to identify the crystalline phases on the membrane upper surface. For XRD analysis, a piece of coated membrane was mounted in horizontal position on the sample stage, grazing incidence mode at 0.5 deg. angle of incidence over a scan 2θ range from 20° to 60°, 40 kV accelerating voltage and 30 mA applied current were used. analysis, a piece of an as produced coated membrane was mounted in horizontal position on the sample stage. Grazing

### 2.3. Photocatalytic activity

The photocatalytic activity was evaluated through methylene blue (MB) photocatalytic decolorization under ultraviolet irradiation (UV). Membranes were placed into crystallization dishes containing a solution of 3.2 mg $L^{-1}$ MB in water and kept in the dark for 24 h to ensure the adsorption equilibrium to be achieved. Next, membranes were transferred to a new 3.2 mg $L^{-1}$ MB solution and exposed to UV light (365 nm, 15 W) for 24 h. The resulting MB decolorization was analysed using a UV–Vis spectrophotometer via absorbance decay measurements. The percentage of MB removal (%MB removal) was calculated as described in Eq. (1)

$$\% \, MB \, removal = (1 - C / C_0). \, 100\% \tag{1}$$

where $C_0$ and C are respectively, the initial and final MB concentration.

### 2.4. Filtration experiments

Membrane filtration tests were performed using a self-made membrane module equipped with a UV LED light (3 W, λ = 365 nm), placed 7 cm above the membrane surface on the permeation side and the flux was set in a cross-flow configuration, with total retentate recycling (Fig. 1). The permeate flux (J) (L $m^{-2} \, h^{-1}$) along the experiments was calculated according to Eq. (2), where V (L) is the permeated volume in a period t (h) through a membrane surface area A (m$^2$).

$$J = \frac{1}{A}.\frac{dV}{dt} \tag{2}$$

The experiments were divided into three different filtration test sets. In the first and second sets, membranes with the thicker $TiO_2$ layers, namely MS-200 nm and MS-400 nm were used to filter a MB solution (3.2 mg $L^{-1}$). Transmembrane pressure (TMP) was set at 0.3 MPa. For the third set, the membrane MS-50 nm was used to filter a soybean oil emulsion (1 g $L^{-1}$) at 0.1 MPa TMP. To produce the oily emulsion, 2 mM of sodium dodecyl sulfate was dissolved in 1 L of deionized water. Then, 1 g of soybean oil was mixed under vigorous magnetic stirring for 5 min, followed by sonication for 5 min. At the end of each experiment, the membrane was kept inside the filled module for 15 h under UV at ambient pressure. No transport of the solution through the membrane
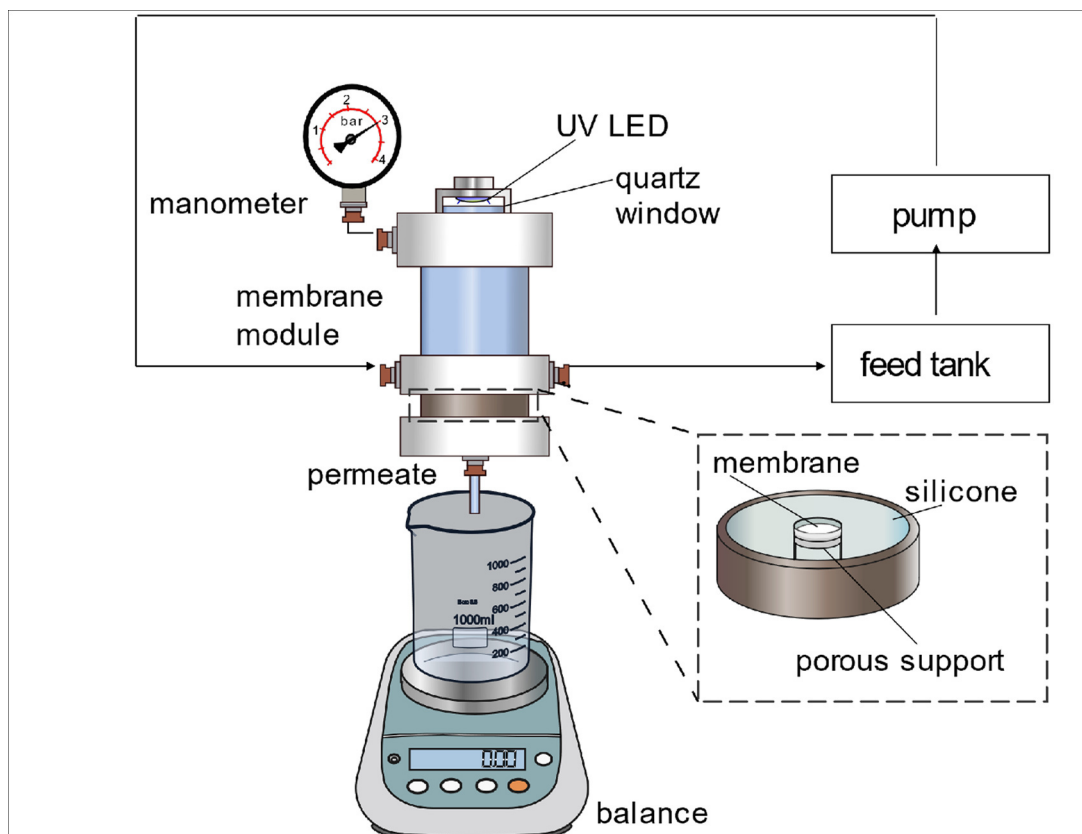
**Fig. 1.** Membrane module.

was observed during this period. Next, without removing the membrane or emptying the module/recirculation tank, TMP was set back to 0.3 MPa (in the case of MB filtration) or 0.1 MPa (in the case of oil emulsion filtration), and a new filtration cycle (2nd cycle) was initiated to evaluate the fouling self-cleaning properties of each membrane/system.

The first filtration test was conducted with the membrane with the thicker TiO$_2$ layer, MS-400 nm, without UV light for 1 h, followed by the 15 h interval under UV. The 2nd cycle was performed under the same conditions as the 1st cycle. For the second filtration test, the membrane MS-200 nm was used. Here, the first filtration cycle was performed without UV light for 45 min, followed by a further 30 min permeation under UV light. TMP was then set to ambient pressure for the 15 h interval under UV before the 2nd cycle was started. For the 2nd filtration cycle, the experiment started once again at 0.3 MPa without UV, which was then turned on after a permeation volume of 5 mL was reached. Permeate MB concentration after each test was obtained through a UV–Vis spectrophotometer and the%MB removal was calculated according to Equation 1.

For the third set, the membrane MS-50 nm was used to filter a soybean oil emulsion (1 g $L^{-1}$) at 0.1 MPa. Three permeate samples were collected after 15, 25, and 35 mL permeate, respectively. After the first sampling, the UV light was switched on. For each permeate sample,% Turbidity removal was calculated according to Eq. (3), where *Turb* and Turb$_0$ are the sampled permeate and feed emulsion turbidity respectively. At the end of the filtration experiment, overall membrane selectivity was evaluated in terms of Total Organic Carbon (TOC) according to Eq. (4), where TOC is the TOC of the filtrate at the end of the experiment and TOC$_0$ refers to the feed emulsion TOC.

$$\%Turb\ removal = \left( 1 - \frac{Turb}{Turb_0} \right) \cdot 100\% \tag{3}$$

$$\%TOC\ removal = \left( 1 - \frac{TOC}{TOC_0} \right) \cdot 100\% \tag{4}$$

## 3. Results and discussion

### 3.1. Membrane morphology and surface chemistry

The coated membrane surfaces have been analyzed by SEM Fig. 2.(a-c) shows SEM images of surface cross-section (50 kx magnification) for uncoated, 50 nm, and 400 nm coated membranes, respectively. A columnar layer of TiO$_2$ on the surface of the membrane can be observed for MS-400 nm membrane (Fig. 2c), displaying a thickness close to 400 nm. Although surface modification can also be observed at MS-50 nm (Fig. 2b), it is less obvious due to the smaller thickness of the coating layer combined with the porous natures of the membranes. Furthermore, a 10kx magnification SEM image of the MS-50 nm (Fig. 2d) revealed the presence of heterogeneity in the membrane surface coverage.

TiO$_2$ coating layers can play different roles. First, TiO$_2$ has been used to improve permeability by improving membrane hydrophilicity and/or producing light-induced hydrophilicity, besides reducing fouling caused by non-polar compounds such as oil molecules. In this case, TiO$_2$ surface coverage can contribute to membrane performance [27,38,39], due to the combined effect of enhanced hydrophilicity and photocatalytic activity under light irradiation. Second, TiO$_2$ can produce photocatalytic membranes, which have been used for photocatalytic degradation of bulk contaminants using immobilized photocatalysts followed by non-simultaneous filtration [40]; to degrade small molecules which cannot be retained during filtration [41]; and, more interestingly, to produce self-cleaning, antifouling membranes and photocatalytic activity under light irradiation [42,43]. In the last case, the homogeneous and complete coverage of the membrane surface with TiO$_2$ is an
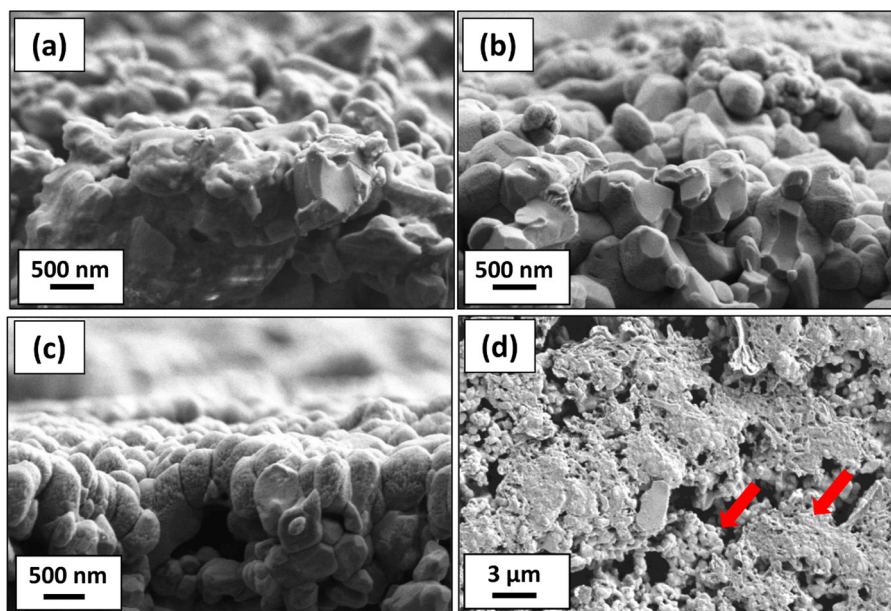
**Fig. 2.** SEM images of surface cross-section (50 kx magnification) before (a) and after film deposition for (b) MS-50 nm and (c) MS-400 nm, and (d) SEM image (10kx) of membrane surface for MS-50 nm, indicating coverage heterogeneity.

important issue.

Finally, coating deposition can be used for pore size tailoring depending on the desired application (particle size of the pollutants) Fig. 3. shows SEM micrographs of the surfaces for the bare membrane (a) and after film deposition for (b) MS-50 nm, (c) MS-200 nm, and (d) MS-400 nm. Membrane surfaces modified by the addition of a TiO$_2$ layer increased in thickness from 50 nm (MS-50 nm) and 200 nm (MS-200 nm) (Fig. 3b-c) when compared to the uncoated membrane (Fig. 3a). When the thickness of the coating layer is further increased to 400 nm (Fig. 3d) no difference is observed anymore compared to the 200 nm coating layer (MS-200 nm).

No significant changes in the pore sizes were observed for the MS-50 nm compared to the bare membrane (Table 1). On the other hand, for the membranes MS-200 nm and MS-400 nm, the deposited layer almost filled the whole surface porosity, when compared to the uncoated

**Table 1**

Average pore size, number of pores counted, and%area occupied by pores from surface image processing (SEM images 5000x magnification) using a dedicated software (ImageJ).

| Membrane | Average pore size (μm) | Counts | % Area occupied by pores |
|---|---|---|---|
| Bare | 0.63 | 535 | 9 |
| MS-50 nm | 0.49 | 531 | 9 |
| MS-200 nm | 0.12 | 1144 | <1 |
| MS-400 nm | 0.14 | 1542 | <1 |

membrane. For these membranes, average pore sizes were reduced to 0.12 μm. Besides, the total membrane area occupied by pores dropped from almost 9% for the bare and MS-50 nm membranes, to less than 1% for MS-200 nm and MS-400 nm. All membranes were in a pore size range
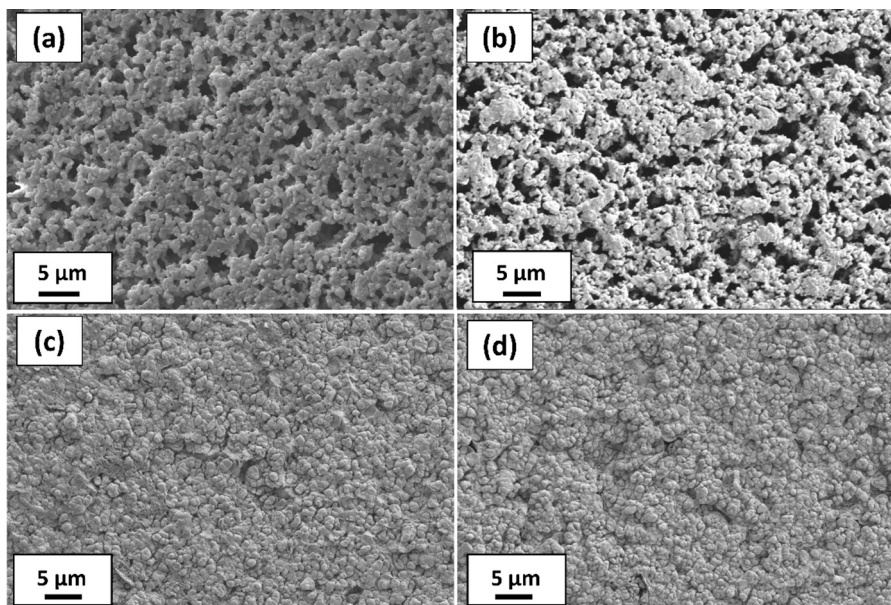


**Fig. 3.** SEM images of membrane surface (5 kx magnification) before (a) and after film deposition for (b) MS-50 nm, (c) MS-200 nm, and (d) MS-400 nm.

(0.62–0.12 μm) suitable for microfiltration, while MS-200 nm and MS-400 nm could also be considered ultrafiltration membranes. This result suggests that magnetron sputtering can be used to produce tailored surface porosity, although further intermediary coating thickness needs to be investigated.

EDS elemental mapping analysis for aluminum (green), oxygen (blue), and titanium (red) were performed using a MS-200 nm membrane, with the SEM image showing both, surface and cross-section portions. (Fig. 4a). While Al and O are well distributed on both sections, the Ti map confirms the presence of Ti homogeneously distributed on the membrane surface. Although the sparse red point indicates the presence of Ti along the membrane cross-section, EDS data for two selected areas (Spectrum 1 and 2 in Fig. 4b) identified the presence of aluminum and oxygen. An element profile (Fig. 4c) was obtained along a data line (Fig. 4b) from the estimated surface to the inside of the membrane through the cross-section. It was possible to confirm that Ti penetrated only a few micrometers (less than 8 μm) inside the membrane pores. The presence of Au visible in Fig. 4c is due to gold sputtering before the SEM images were taken.

Titania in the anatase phase was formed on coated membrane surfaces according to Raman spectrum (Fig. 5a) and further confirmed by XRD (Fig. 5b), while no rutile peaks were found. Additionally, a significant increase in anatase peaks was observed in the XRD patterns of the coating from 50 to 400 nm coatings.

### 3.2. Photocatalytic activity

UV energy can degrade some compounds due to photolysis reactions, even in absence of photocatalysts. Thus, to prove the MB solution discoloration is due to photocatalysis, experiments in the absence of membranes in the MB-containing solution were carried out before the photocatalytic experiments. MB photolysis degradation was lower than 2% under the experimental conditions used in this study. Photocatalytic tests showed photocatalytic active layers were produced. While for bare membranes less than 2% MB removal (due to photolysis) was achieved, this amount was much higher - 21 and 26% - for MS-50 nm and MS-200 nm membranes, respectively. It is also worth mentioning that an increase of 4x on TiO2 layer thickness led to only a 4% improvement in MB removal efficiency. The small increase in MB removal can be explained by the fact that photocatalysis is a surface phenomenon that requires surface irradiation [24]. It has been shown that the light can penetrate deep and activate $TiO_2$ when the layer is very thin. Using a radiant flux of 3.48 mW cm$^{-2}$, photo-generated electrons and holes were formed mainly on $TiO_2$ films with a surface depth of around 30 nm. A further increase of the $TiO_2$ film thickness had a minor influence on photocatalytic activity [20].

### 3.3. Methylene blue filtration

MS-400 nm and MS-200 nm membranes were used in the first and second sets of filtration experiments, respectively. When comparing the thicker membrane (Fig. 6a) to the second one (Fig. 6b), the permeation flux was significantly lower. The higher flux is due to the thinner coating layers on MS-200 nm, which reduces flux resistance. Despite that, the membrane MS-400 nm demonstrated high MB selectivity, removing approximately 86% of MB from the permeate. In the MS-200 nm,
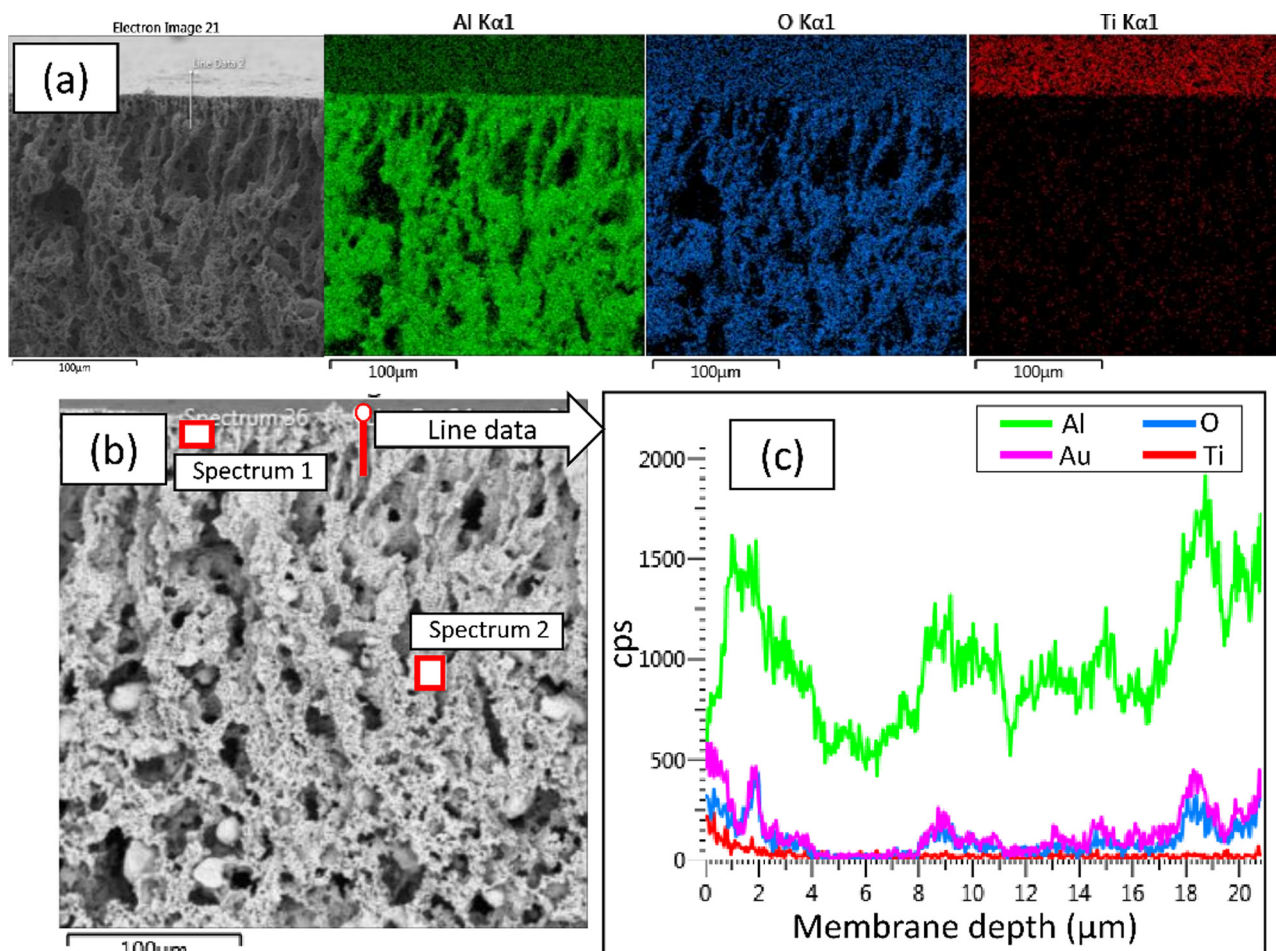


**Fig. 4.** (a) Color mapping for aluminum, oxygen, and titanium of a MS-200 nm membrane, (b) near-surface cross-section SEM image of a MS-200 nm membrane with selected two areas (spectrum 1 and 2) and a line for EDS analysis, and (c) element data along the selected line.
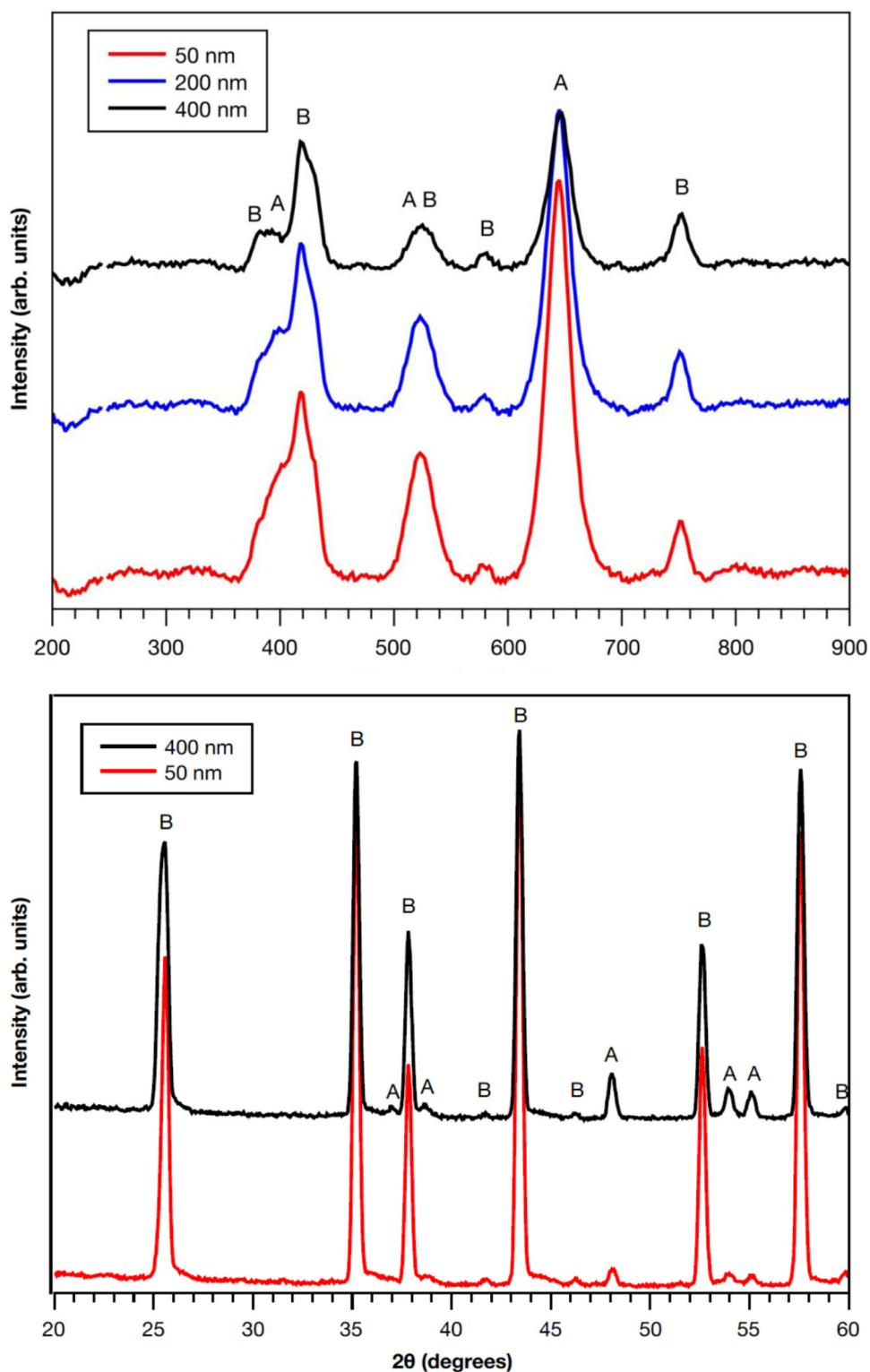
**Fig. 5.** Raman (a) and XRD pattern (b) for produced membranes. Peaks assigned as "A" refer to anatase phase of $TiO_2$, "B" refers to $\alpha$-$Al_2O_3$.

membrane selectivity fell to 66.5% MB elimination, a 20% reduction in selectivity.

Flux decline along filtration experiments for both MS-400 nm (Fig. 6a) and MS-200 nm (Fig. 6b) membranes are attributed to fouling formation. Fouling can be formed on the membrane surface or inside the pores, depending on the fouling mechanism as described by Hermia's law [44]. A fouling layer on a membrane surface is called cake and may happen regardless of the formation of fouling inside the pores. The main

influence on fouling in the pores is the ratio between pore and pollutant size. Membranes with smaller relative pore sizes present higher selectivity and are more likely to foul only or mainly at the surface. Since fouling is a normal phenomenon in membrane processes, cleaning pause procedures are necessary. Thus, physical cleaning or/and chemical cleaning methods have been applied for this purpose, where irreversible residual contamination is still to be expected [45].

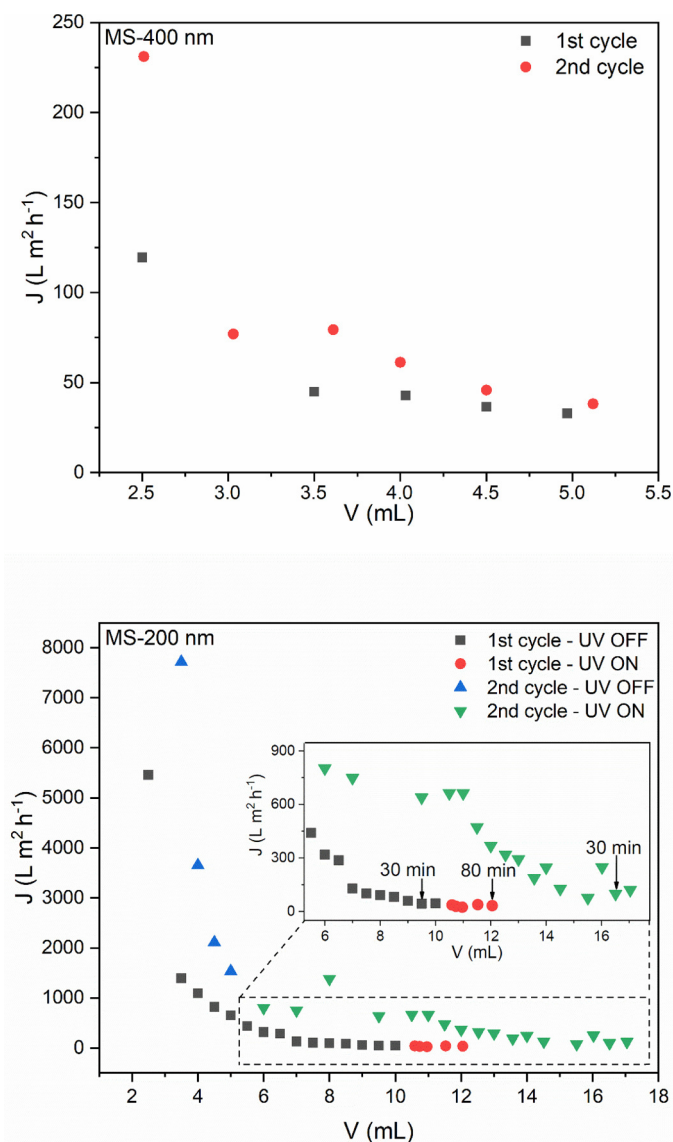Membranes containing photocatalytic surfaces under suitable

**Fig. 6.** Permeate flux and the respective permeate volumes for (a) MS-400 nm and (b) MS-200 nm (insert with a zoom between 5.5 and 18 mL) membranes during filtration of a methylene blue solution 3.2 mg $L^{-1}$ under 0.3 MPa for two filtration cycles, with an interval of 15 h under UV.

radiation have been reported to improve membrane cleaning performance and reduce irreversible fouling without the necessity of adding chemicals [46,47]. In this work, membranes were capable of completely recovering MB flux after UV treatment (15 h interval under UV after the 1st filtration cycle) and the second cycle showed a similar behavior compared to the 1st cycle (Fig. 6a and Fig. 6b). Since the module was kept filled during the 15-hour UV irradiation, the higher initial flux values for the second cycle can be due to a slightly lower concentration of the MB solution within the module at the start of the second cycle. It should be noted that only the surface of the membranes produced contains photocatalyst, which means that only surface fouling can be photocatalytically decomposed under UV irradiation. The complete recovery of flux for both membranes indicates that fouling has formed mainly on the membrane surface, while the selectivity of the membranes indicates that fouling can also be formed inside the pores when MB is filtrated.

The 1st cycle using MS-200 nm was performed without UV light for the first 10 mL permeate (45 min), after which the flux rate was already very low (Fig. 6b – 1st cycle – UV OFF). Next, UV light was switched on

and flux was recorded for a further 30 min (around 2 mL of permeate). Nonetheless, in contrast to the 15 h UV treatment, no increment in the flux J was observed during this period (Fig. 6b – 1st cycle – UV ON).

Since photocatalysis is a surface reaction, an excess of foulant will slow down the reaction rate by preventing light from reaching the membrane surface. To investigate this influence, the UV light was turned on earlier for the second filtration cycle, after a permeation volume of 5 mL had been achieved. Up to a permeate volume of 10 mL permeation, a slight flux recovery was observed, with a flux drop rate attenuation. The oscillation of the flux during the UV irradiation period (inset in Fig. 6b) was attributed to the degradation reactions of the fouling, which almost doubled the permeation volume in the same time range. After a certain period, the UV light could no longer maintain or reduce the flux drop during filtration (Fig. 6b). This can happen when the deposition rate of the fouling on the membrane surface is faster than the degradation reaction [48]. In this context, surface fouling deposition can extend operation periods between fouling intervals when optimized conditions are used.

### 3.4. Oily emulsion filtration

The membrane with the thinner titania layer, MS-50 nm, possesses an average pore size suitable only for microfiltration. Oily wastewater is an important global issue and its treatment by photocatalysis, micro, and ultra-filtration treatment have received increasing interest, while the application of photocatalytic membrane for this purpose is still scarce [9,27,56,40,17,49–55]. Thus, filtration of a soybean oil emulsion (1 g $L^{-1}$) at 0.1 MPa was chosen as the target pollutant to evaluate this membrane.

Three samples were collected after 15, 25, and 35 mL permeate, respectively. After the first sampling, UV light was turned on (Fig. 7). At the end of the experiment, an overall TOC removal of 60% was achieved, while turbidity removal was 85.5, 95, and 96% for the first, second, and third sampling, respectively. Turbidity removal increases were attributed to pore narrowing due to the deposition of foulants on the membrane or inside the pores [56]. Despite the selectivity results, no flux recovery or flux drop rate attenuation was observed during the experiments with oily wastewater under UV (Fig. 7). Also, differently from the MB filtration experiments, no flux recovery was observed after the 15 h UV interval under UV. To confirm this effect, the membrane module was again kept overnight under UV irradiation at ambient pressure to provide long-term irradiation on the membrane surface. Still, no fouling
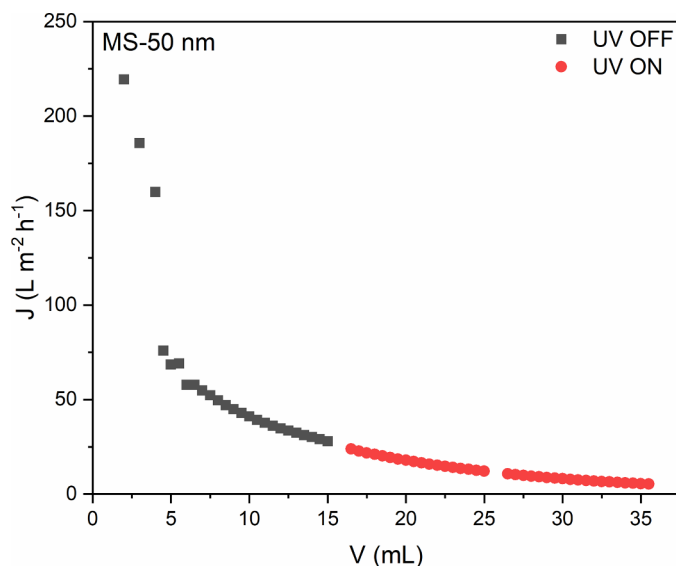


**Fig. 7.** Permeate flux and the respective permeate volumes for MS-50 nm during a 1 g $L^{-1}$ oily emulsion filtration at 0.1 MPa.

recovery was observed. For this reason, it was not possible to perform a 2nd filtration cycle in this case.

The lack of flux recovery is driven by two main factors. Firstly, the membrane has separated 60% of the feed oil. This means that some of the oil has passed through the membrane pores and deposited inside the pores. Although batch photocatalyst tests (Section 3.2) have shown similar photocatalytic capabilities for MS-50 nm and MS-200 nm membranes, the photocatalytic surface layer of the membrane is not able to decompose fouling inside the pores. In this case, the question arises as to the pore size of the membrane, whereby filtration performance could be improved by using a bare membrane with narrower pore sizes (improving selectivity), while 50 nm coating layer can solely play the role of surface functionalization (photocatalysis). Secondly, photocatalysis is a surface reaction. Thick layers of foulant compounds deposited on the membrane surface during the filtration can hinder the proper irradiation of the photocatalytic surface. Also, if the degradation mechanism is indirect oxidation (by hydroxil and superoxide radicals) and the $TiO_2$ layer is completely insulated with oil, the radical formation can be hindered by the lack of sufficient oxygen on the membrane surface [27,57]. A membrane module equipped with more intense light irradiation could improve the photocatalytic reaction rate to a certain degree, which could improve the antifouling properties of the membrane and increase the duration of the filtration cycle [48,58].

## 4. Conclusions

Photocatalytic ceramic membranes suitable for micro- or ultrafiltration processes with tailored surface porosity and using a UV light for MB removal were produced by $TiO_2$ deposition by magnetron sputtering. High selectivity and self-cleaning properties were obtained. An anatase coating layer was formed on the membrane surfaces and the coating thickness was a major influence on selectivity, but a minor effect on photocatalytic activity. Only 4% more MB removal was obtained when the $TiO_2$ coating layer was increased by 4 times (from 50 to 200 nm). Higher flux can be obtained in the early presence of UV light, while the light has little online effect on flux when a thick fouling layer has been formed. An extended UV exposure was able to recover the MB flux. Under the conditions used, degradation of soybean oil could not be observed. Further investigation is required to improve the antifouling properties for oily wastewater filtration. Finally, magnetron sputtering is a versatile technique, future work can also involve the deposition of different photocatalysts to produce active layers under visible light.

## CRediT authorship contribution statement

**Leticya Lais Coelho:** Validation, Investigation, Writing – original draft, Formal analysis, Writing – review & editing. **Matthieu Grao:** Validation, Investigation, Writing – original draft, Writing – review & editing. **Thomas Pomone:** Validation, Investigation, Formal analysis. **Marina Ratova:** Formal analysis, Methodology, Writing – original draft, Supervision, Writing – review & editing. **Peter Kelly:** Formal analysis, Supervision, Writing – review & editing. **Michaela Wilhelm:** Formal analysis, Methodology, Writing – original draft, Supervision, Writing – review & editing. **Regina de Fátima Peralta Muniz Moreira:** Conceptualization, Methodology, Formal analysis, Resources, Writing – review & editing, Supervision, Project administration.

## Declaration of Competing Interest

None.

## Acknowledgments

## References

[1] M. Kamali, D.P. Suhas, M.E. Costa, I. Capela, T.M. Aminabhavi, Sustainability considerations in membrane-based technologies for industrial effluents treatment, Chem. Eng. J. (2019), https://doi.org/10.1016/j.cej.2019.02.075.

[2] S.P. Dharupaneedi, S.K. Nataraj, M. Nadagouda, K.R. Reddy, S.S. Shukla, T. M. Aminabhavi, Membrane-based separation of potential emerging pollutants, Sep. Purif. Technol. 210 (2019) 850–866, https://doi.org/10.1016/j.seppur.2018.09.003.

[3] S. Leong, A. Razmjou, K. Wang, K. Hapgood, X. Zhang, H. Wang, TiO2 based photocatalytic membranes: a review, J. Memb. Sci. 472 (2014) 167–184, https://doi.org/10.1016/j.memsci.2014.08.016.

[4] G. Mustafa, K. Wyns, A. Buekenhoudt, V. Meynen, Antifouling grafting of ceramic membranes validated in a variety of challenging wastewaters, Water Res 104 (2016) 242–253, https://doi.org/10.1016/j.watres.2016.07.057.

[5] R. Molinari, C. Lavorato, P. Argurio, Recent progress of photocatalytic membrane reactors in water treatment and in synthesis of organic compounds. A review, Catal. Today. 281 (2017) 144–164, https://doi.org/10.1016/j.cej.2015.03.120.

[6] L.T. Nyamutswa, B. Zhu, S.F. Collins, D. Navaratna, M.C. Duke, Light conducting photocatalytic membrane for chemical-free fouling control in water treatment, J. Memb. Sci. 604 (2020), 118018, https://doi.org/10.1016/j.memsci.2020.118018.

[7] M. Padaki, R.S. Murali, M.S. Abdullah, N. Misdan, A. Moslehyani, M.A. Kassim, N. Hilal, A.F. Ismail, Membrane technology enhancement in oil-water separation: a review, Des 357 (2015) 197–207, https://doi.org/10.1016/j.desal.2014.11.023.

[8] C. Byrne, G. Subramanian, S.C. Pillai, Recent advances in photocatalysis for environmental applications, J. Environ. Chem. Eng. 6 (2018) 3531–3555, https://doi.org/10.1016/j.jece.2017.07.080.

[9] P.C. Silva, N.P. Ferraz, E.A. Perpetuo, Y.J.O. Asencios, Treatment of oil produced water using advanced oxidative processes: heterogeneous-photocatalysis and photo-fenton, Environ. Div. 2018 - core program. area 2018, AIChE Annu. Meet. 4 (2018) 35–37, https://doi.org/10.12957/jse.2019.40991.

[10] D. Ma, H. Yi, C. Lai, X. Liu, X. Huo, Z. An, L. Li, Y. Fu, B. Li, M. Zhang, L. Qin, S. Liu, L. Yang, Critical review of advanced oxidation processes in organic wastewater treatment, Chemosphere 275 (2021), 130104, https://doi.org/10.1016/j.chemosphere.2021.130104.

[11] X. Chen, Y. Hu, Z. Xie, H. Wang, Materials and Design of Photocatalytic Membranes, Elsevier Inc., 2018, https://doi.org/10.1016/B978-0-12-813549-5.00003-7.

[12] S. Samsami, M. Mohamadi, M.H. Sarrafzadeh, E.R. Rene, M. Firoozbahr, Recent advances in the treatment of dye-containing wastewater from textile industries: overview and perspectives, Process Saf. Environ. Prot. 143 (2020) 138–163, https://doi.org/10.1016/j.psep.2020.05.034.

[13] N. Nasrollahi, L. Ghalamchi, V. Vatanpour, A. Khataee, Photocatalytic-membrane technology: a critical review for membrane fouling mitigation, J. Ind. Eng. Chem. 93 (2020) 101–116, https://doi.org/10.1016/j.jiec.2020.09.031.

[14] S. Mozia, Photocatalytic membrane reactors (PMRs) in water and wastewater treatment. A review, Sep. Purif. Technol. 73 (2010) 71–91, https://doi.org/10.1016/j.seppur.2010.03.021.

[15] M. Lee, Z. Wu, K. Li, Advances in ceramic membranes for water treatment, 2015. https://doi.org/10.1016/B978-1-78242-121-4.00002-2.

[16] N.F.D. Junaidi, N.H. Othman, N.S. Fuzil, M.S. Mat Shayuti, N.H. Alias, M. Z. Shahruddin, F. Marpani, W.J. Lau, A.F. Ismail, N.F.D. Aba, Recent development of graphene oxide-based membranes for oil-water separation: a review, Sep. Purif. Technol. 258 (2021), 118000, https://doi.org/10.1016/j.seppur.2020.118000.

[17] D. Zhang, G. Wang, S. Zhi, K. Xu, L. Zhu, W. Li, Z. Zeng, Q. Xue, Superhydrophilicity and underwater superoleophobicity TiO2 /Al2O3 composite membrane with ultralow oil adhesion for highly efficient oil-in-water emulsions separation, Appl. Surf. Sci. 458 (2018) 157–165, https://doi.org/10.1016/j.apsusc.2018.07.052.

[18] I. Horovitz, I. Horovitz, V. Gitis, D. Avisar, H. Mamane, Ceramic-based photocatalytic membrane reactors for water treatment - where to next? Rev. Chem. Eng. 36 (2020) 593–622, https://doi.org/10.1515/revce-2018-0036.

[19] S. Riaz, S.J. Park, An overview of TiO2-based photocatalytic membrane reactors for water and wastewater treatments, J. Ind. Eng. Chem. 84 (2020) 23–41, https://doi.org/10.1016/j.jiec.2019.12.021.

[20] H. Choi, E. Stathatos, D.D. Dionysiou, Sol-gel preparation of mesoporous photocatalytic TiO2 films and TiO2/Al2O3 composite membranes for environmental applications, Appl. Catal. B Environ. 63 (2006) 60–67, https://doi.org/10.1016/j.apcatb.2005.09.012.

[21] T. Yang, F. Liu, H. Xiong, Q. Yang, F. Chen, C. Zhan, Fouling process and anti-fouling mechanisms of dynamic membrane assisted by photocatalytic oxidation under sub-critical fluxes, Chinese J. Chem. Eng. 27 (2019) 1798–1806, https://doi.org/10.1016/j.cjche.2018.10.019.

[22] A. Moslehyani, S.K. Hubadillah, M. Hafiz, D. Othman, A.F. Ismail, T. Matsuura, Contaminants: water and wastewater treatment, (2018) 189–208.

[23] L. Chen, P. Xu, H. Wang, Photocatalytic membrane reactors for produced water treatment and reuse: fundamentals, affecting factors, rational design, and evaluation metrics, J. Hazard. Mater. 424 (2022), 127493, https://doi.org/10.1016/j.jhazmat.2021.127493.

[24] A. Fujishima, X. Zhang, D.A. Tryk, TiO$_2$ photocatalysis and related surface phenomena, Surf. Sci. Rep. 63 (2008) 515–582, https://doi.org/10.1016/j.surfrep.2008.10.001.

[25] C.P. Athanasekou, N.G. Moustakas, S. Morales-Torres, L.M. Pastrana-Martínez, J.L. Figueiredo, J.L. Faria, A.M.T. Silva, J.M. Dona-Rodriguez, G.E. Romanos, P. Falaras, Ceramic photocatalytic membranes for water filtration under UV and visible light, Appl. Catal. B Environ. 178 (2014) 12–19, https://doi.org/10.1016/j.apcatb.2014.11.021.

[26] N.E. Salim, J. Jaafar, A.F. Ismail, M.H.D. Othman, M.A. Rahman, N. Yusof, M. Qtaishat, T. Matsuura, F. Aziz, W.N.W. Salleh, Preparation and characterization of hydrophilic surface modifier macromolecule modified poly (ether sulfone) photocatalytic membrane for phenol removal, Chem. Eng. J. 335 (2018) 236–247, https://doi.org/10.1016/j.cej.2017.10.147.c.

[27] A. Golshenas, Z. Sadeghian, S.N. Ashrafizadeh, Performance evaluation of a ceramic-based photocatalytic membrane reactor for treatment of oily wastewater, J. Water Process Eng. 36 (2020), 101186, https://doi.org/10.1016/j.jwpe.2020.101186.

[28] H. Salazar, P.M. Martins, B. Santos, M.M. Fernandes, A. Reizabal, V. Sebastián, G. Botelho, C.J. Tavares, J.L. Vilas-Vilela, S. Lanceros-Mendez, Photocatalytic and antimicrobial multifunctional nanocomposite membranes for emerging pollutants water treatment applications, Chemosphere (2020) 250, https://doi.org/10.1016/j.chemosphere.2020.126299.

[29] Y.X. Li, P. Li, Y.Z. Wu, Z.L. Xu, M.L. Huang, Preparation and antifouling performance of thin inorganic ultrafiltration membrane via assisted sol-gel method with different composition of dual additives, Ceram. Int. (2020), https://doi.org/10.1016/j.ceramint.2020.09.056.

[30] B.J. Starr, V.V. Tarabara, M. Zhou, S. Roualdès, A. Ayral, Coating porous membranes with a photocatalyst: comparison of LbL self-assembly and plasma-enhanced CVD techniques, J. Memb. Sci. 514 (2016) 340–349, https://doi.org/10.1016/j.memsci.2016.04.050.

[31] S. Sanches, C. Nunes, P.C. Passarinho, F.C. Ferreira, V.J. Pereira, J.G. Crespo, Development of photocatalytic titanium dioxide membranes for degradation of recalcitrant compounds, J. Chem. Technol. Biotechnol. 92 (2017) 1727–1737, https://doi.org/10.1002/jctb.5172.

[32] P.J. Kelly, R.D. Arnell, Magnetron sputtering: a review of recent developments and applications, 56 (2000) 159–172. https://doi.org/10.1016/S0042-207X(99)00189-X.

[33] M. Ratova, P.J. Kelly, G.T. West, X. Xia, Y. Gao, deposition of visible light active photocatalytic bismuth molybdate thin films by reactive magnetron sputtering, (2016). https://doi.org/10.3390/ma9020067.

[34] S. Khamseh, F. Abdollahzadeh Davani, A. Samimi, The effects of RF-sputtered TiO$_2$ top layer on pore structure of composite ceramic membranes, Surf. Coatings Technol. 258 (2014) 1256–1258, https://doi.org/10.1016/j.surfcoat.2014.07.014.

[35] R. Bergamasco, F.V. da Silva, F.S. Arakawa, N.U. Yamaguchi, M.H.M. Reis, C.J. Tavares, M.T.P.S. de Amorim, C.R.G. Tavares, Drinking water treatment in a gravimetric flow system with TiO$_2$ coated membranes, Chem. Eng. J. 174 (2011) 102–109, https://doi.org/10.1016/j.cej.2011.08.056.

[36] L.L. Coelho, M. Di Luccio, D. Hotza, R. de Fátima Peralta Muniz Moreira, A.C. Moreira, C.P. Fernandes, K. Rezwan, M. Wilhelm, Tailoring asymmetric Al$_2$O$_3$ membranes by combining tape casting and phase inversion, J. Memb. Sci. 623 (2021), 119056, https://doi.org/10.1016/j.memsci.2021.119056.

[37] J. Sakaliuniene, B. Abakevičiene, K. Šlapikas, S. Tamulevičius, Influence of magnetron sputtering deposition conditions and thermal treatment on properties of platinum thin films for positive electrode-electrolyte-negative electrode structure, Thin Solid Films 594 (2015) 101–108, https://doi.org/10.1016/j.tsf.2015.10.016.

[38] M.A. Henderson, A surface science perspective on TiO2 photocatalysis, 66 (2011) 185–297. https://doi.org/10.1016/j.surfrep.2011.01.001.

[39] S. Huang, R.H.A. Ras, X. Tian, Antifouling membranes for oily wastewater treatment: interplay between wetting and membrane fouling, Curr. Opin. Colloid Interface Sci. 36 (2018) 90–109, https://doi.org/10.1016/j.cocis.2018.02.002.

[40] A. Moslehyani, M. Mobaraki, T. Matsuura, A.F. Ismail, M.H.D. Othman, M.N.K. Chowdhury, Novel green hybrid processes for oily water photooxidation and purification from merchant ship, Desalination 391 (2016) 98–104, https://doi.org/10.1016/j.desal.2016.01.003.

[41] C. Li, Z. Lu, X. Ao, W. Sun, X. Huang, Degradation kinetics and removal efficiencies of pharmaceuticals by photocatalytic ceramic membranes using ultraviolet light-emitting diodes, Chem. Eng. J. 427 (2022), 130828, https://doi.org/10.1016/j.cej.2021.130828.

[42] N.T. Padmanabhan, H. John, Titanium dioxide based self-cleaning smart surfaces: a short review, J. Environ. Chem. Eng. 8 (2020), 104211, https://doi.org/10.1016/j.jece.2020.104211.

[43] J. Hu, Y. Zhan, G. Zhang, Q. Feng, W. Yang, Y.H. Chiao, S. Zhang, A. Sun, Durable and super-hydrophobic/underwater super-oleophobic two-dimensional MXene composite lamellar membrane with photocatalytic self-cleaning property for efficient oil/water separation in harsh environments, J. Memb. Sci. 637 (2021), 119627, https://doi.org/10.1016/j.memsci.2021.119627.

[44] W. Zhang, L. Ding, Investigation of membrane fouling mechanisms using blocking models in the case of shear-enhanced ultrafiltration, Sep. Purif. Technol. 141 (2015) 160–169, https://doi.org/10.1016/j.seppur.2014.11.041.

[45] W. He, H. Huang, J. fen Gao, L. Winnubst, C. sheng Chen, Phase-inversion tape casting and oxygen permeation properties of supported ceramic membranes, J. Memb. Sci. 452 (2014) 294–299, https://doi.org/10.1016/j.memsci.2013.09.063.

[46] Y. Shi, J. Huang, G. Zeng, W. Cheng, J. Hu, Photocatalytic membrane in water purification: is it stepping closer to be driven by visible light? J. Memb. Sci. 584 (2019) 364–392, https://doi.org/10.1016/j.memsci.2019.04.078.

[47] E.N. Santos, Á. Ágoston, S. Kertész, C. Hodúr, Z. László, Z. Pap, Z. Kása, T. Alapi, S.A.G. Krishnan, G. Arthanareeswaran, K. Hernadi, G. Veréb, Investigation of the applicability of TiO$_2$, BiVO$_4$, and WO$_3$ nanomaterials for advanced photocatalytic membranes used for oil-in-water emulsion separation, Asia-Pacific J. Chem. Eng. 15 (2020) 1–15, https://doi.org/10.1002/apj.2549.

[48] W. Zhang, L. Ding, J. Luo, M.Y. Jaffrin, B. Tang, Membrane fouling in photocatalytic membrane reactors (PMRs) for water and wastewater treatment: a critical review, Chem. Eng. J. 302 (2016) 446–458, https://doi.org/10.1016/j.cej.2016.05.071.

[49] L. Zhu, M. Chen, Y. Dong, C.Y. Tang, A. Huang, A low-cost mullite-titania composite ceramic hollow fiber microfiltration membrane for highly efficient separation of oil-in-water emulsion, Water Res 90 (2016) 277–285, https://doi.org/10.1016/J.WATRES.2015.12.035.

[50] P. Monash, G. Pugazhenthi, Effect of TiO$_2$ addition on the fabrication of ceramic membrane supports: a study on the separation of oil droplets and bovine serum albumin (BSA) from its solution, Desalination 279 (2011) 104–114, https://doi.org/10.1016/j.desal.2011.05.065.

[51] L. Yu, M. Kanezashi, H. Nagasawa, T. Tsuru, Phase inversion/sintering-induced porous ceramic microsheet membranes for high-quality separation of oily wastewater, J. Memb. Sci. 595 (2020), 117477, https://doi.org/10.1016/j.memsci.2019.117477.

[52] N. Yaacob, G.P. Sean, N.A.M. Nazri, A.F. Ismail, M.N. Zainol Abidin, M.N. Subramaniam, Simultaneous oily wastewater adsorption and photodegradation by ZrO$_2$–TiO$_2$ heterojunction photocatalysts, J. Water Process Eng. (2020), 101644, https://doi.org/10.1016/j.jwpe.2020.101644.

[53] M. D'Auria, L. Emanuele, R. Racioppi, V. Velluzzi, Photochemical degradation of crude oil: comparison between direct irradiation, photocatalysis, and photocatalysis on zeolite, J. Hazard. Mater. 164 (2009) 32–38, https://doi.org/10.1016/j.jhazmat.2008.07.111.

[54] C.S. Ong, W.J. Lau, P.S. Goh, B.C. Ng, A.F. Ismail, Investigation of submerged membrane photocatalytic reactor (sMPR) operating parameters during oily wastewater treatment process, 353 (2014) 48–56. https://doi.org/10.1016/j.desal.2014.09.008.

[55] N.H. Alias, J. Jaafar, S. Samitsu, N. Yusof, M.H.D. Othman, M.A. Rahman, A.F. Ismail, F. Aziz, W.N.W. Salleh, N.H. Othman, Photocatalytic degradation of oilfield produced water using graphitic carbon nitride embedded in electrospun polyacrylonitrile nanofibers, Chemosphere 204 (2018) 79–86, https://doi.org/10.1016/j.chemosphere.2018.04.033.

[56] E. Iritani, A review on modeling of pore-blocking behaviors of membranes during pressurized membrane filtration, Dry. Technol. 31 (2013) 146–162, https://doi.org/10.1080/07373937.2012.683123.

[57] M. Grao, M. Ratova, C.C. Amorim, R.B.P. Marcelino, P. Kelly, Crystalline TiO$_2$ supported on stainless steel mesh deposited in a one step process via pulsed DC magnetron sputtering for wastewater treatment applications, J. Mater. Res. Technol. 9 (2020) 5761–5773, https://doi.org/10.1016/j.jmrt.2020.03.101.

[58] J.M. Herrmann, Photocatalysis fundamentals revisited to avoid several misconceptions, Appl. Catal. B Environ. 99 (2010) 461–468, https://doi.org/10.1016/j.apcatb.2010.05.012.

[59] S.M Samaei, S. Gato-Trinidad, A. Altaee, The application of pressure-driven ceramic membrane technology for the treatment of industrial wastewaters – A review, Purif. Technol. (2018), https://doi.org/10.1016/j.seppur.2018.02.041.

[60] M.N. Subramaniam, P. Goh, W. Lau, B. Ng, Chapter 3 - Development of nanomaterial-based photocatalytic membrane for organic pollutants removal, Elsevier, Elsevier Inc., 2019, https://doi.org/10.1016/B978-0-12-814503-6.00003-3.